Marine and Petroleum Geology 148 (2023) 105970

Contents lists available at ScienceDirect

Marine and Petroleum Geology

journal homepage: www.elsevier.com/locate/marpetgeo

Deep fluids migration and submarine emersion of the Kalang Anyar mud volcano (Java, Indonesia): A multidisciplinary study

Adriano Mazzini [a,b,*], Alessandra Sciarra [b], Matteo Lupi [c], Philippa Ascough [d], Grigorii Akhmanov [e], Karyono Karyono [f], Alwi Husein [g]

[a] center for Earth Evolution and Dynamics (CEED), University of Oslo, Oslo, Norway
[b] Istituto Nazionale di Geofisica e Vulcanologia (INGV), Sezione Roma 1, Italy
[c] Department of Earth Sciences, University of Geneva, Switzerland
[d] NEIF Radiocarbon Laboratory, Scottish Universities Environmental Research center, East Kilbride, UK
[e] Faculty of Geology, Lomonosov Moscow State University, Moscow, Russian Federation
[f] Agency for Meteorology, Climatology and Geophysics (BMKG), Jakarta, Indonesia
[g] Pusat Pengendalian Lumpur Sidoarjo (PPLS), Sidoarjo, Indonesia

ARTICLE INFO

Keywords:
Kalang Anyar mud volcano
Methanogenic carbonates
Methane flux quantifications
Seismometers signals
Onshore-offshore seepage
Java-Indonesia

ABSTRACT

North-east Java is part of a large sedimentary basin containing hydrocarbon provinces that feature diffuse hydrothermal systems, mud volcanoes, and degassing sites. Seismic profiles acquired to explore the basin reveal a broad distribution of palaeo- and modern piercement structures. The Watukosek fault system links the volcanic arc, to the south, with the Sidoarjo province, to the north. Several piercement structures, including the Kalang Anyar mud volcano, are hosted along this left-lateral strike-slip system that favors the migration of crustal fluids in this part of the basin. Here, we present a multidisciplinary geological, geophysical and geochemical study conducted at Kalang Anyar where dozens of seepage sites are active in the crater area and intermittently emit bursts oil, gas, mud, and water. The emitted gasses are methane-dominated with smaller amounts of heavier hydrocarbons and CO_2. Unlike most mud volcanoes, at Kalang Anyar the mixed-thermogenic origin of the methane is coupled with geothermal anomalies, as indicated by helium and CO_2 isotopic values ($\delta^{13}C_{CO2}$ as high as −4‰) that suggest the input of mantle-derived gas. Our gas flux measurements reveal that Kalang Anyar emits about 1.62 and 5.75 t yr^{-1} of CO_2 and CH_4, respectively. The intense bubbling gives rise to a typical drumbeat seismic signal characterized by dominant frequencies around of 3–4 Hz (and up to 15 Hz). We interpret the drumbeat as fluids rising and resonating through shallow plumbing system of Kalang Anyar. Erupted clasts with different lithologies and shells are scattered across the mud volcano area, while the edges of the crater zone include cubic meter-sized carbonate-cemented blocks and ridges that contain siliciclastic sediments and abundant chemosymbiotic bivalves. Carbon isotope analyses of the carbonate cement ($\delta^{13}C$ as low as −48.8‰) identify the latter as methanogenic chemoherms. Radiocarbon (^{14}C) dating of bivalves cemented in the blocks indicates an age of 1890-1488 BP. These results indicate that the activity of Kalang Anyar MV dates from when the area was below sea level and that the microbially-mediated precipitation of carbonates was ongoing during subaqueous methane seepage at the crater site.

To the best of our knowledge, Kalang Anyar is the first example of a mud volcano that progressed from subaqueous to subaerial conditions during marine regression, displaying evidence of former marine activity (i.e. methanogenic carbonates) and current subaerial degassing at numerous seepage sites. Potentially eruptive phases represent a clear geohazard for the numerous settlements constructed inside the mud volcano. In light of this, it may be prudent to apply stricter rules for development activities, such as housing construction permits that consider the possibility of potentially catastrophic events, and apply steps to mitigate these hazards.

* Corresponding author. center for Earth Evolution and Dynamics (CEED), University of Oslo, Oslo, Norway.
E-mail address: adriano.mazzini@geo.uio.no (A. Mazzini).

https://doi.org/10.1016/j.marpetgeo.2022.105970
Received 24 March 2022; Received in revised form 5 October 2022; Accepted 8 October 2022
Available online 13 October 2022

1. Introduction

The north-eastern part of the island of Java is part of a back-arc basin containing a petroleum province that is characterized by numerous modern and palaeo-piercement structures (e.g. mud volcanoes, buried vents, and diapirs). The region contains evidence of extensive interactions between gravitatively-unstable buoyant shales, faulting, hydrothermal activity, and hydrocarbons generation (Mazzini et al., 2007; Satyana and Asnidar, 2008; Istadi et al., 2012; Moscariello et al., 2018; Zaputlyaeva et al., 2020). North East Java hosts at least six dormant mud volcanoes (MVs), as well as several buried palaeo-vents and diapirs (Miller and Mazzini, 2018). This part of the back-arc basin is connected to the Arjuno-Welirang volcanic complex by the left-lateral Watukosek Fault System (WFS) (Mazzini et al., 2009; Fallahi et al., 2017; Moscariello et al., 2018; Sciarra et al., 2018; Lupi et al., 2022). The authors describe the main features of the WFS observed in the seismic data, and

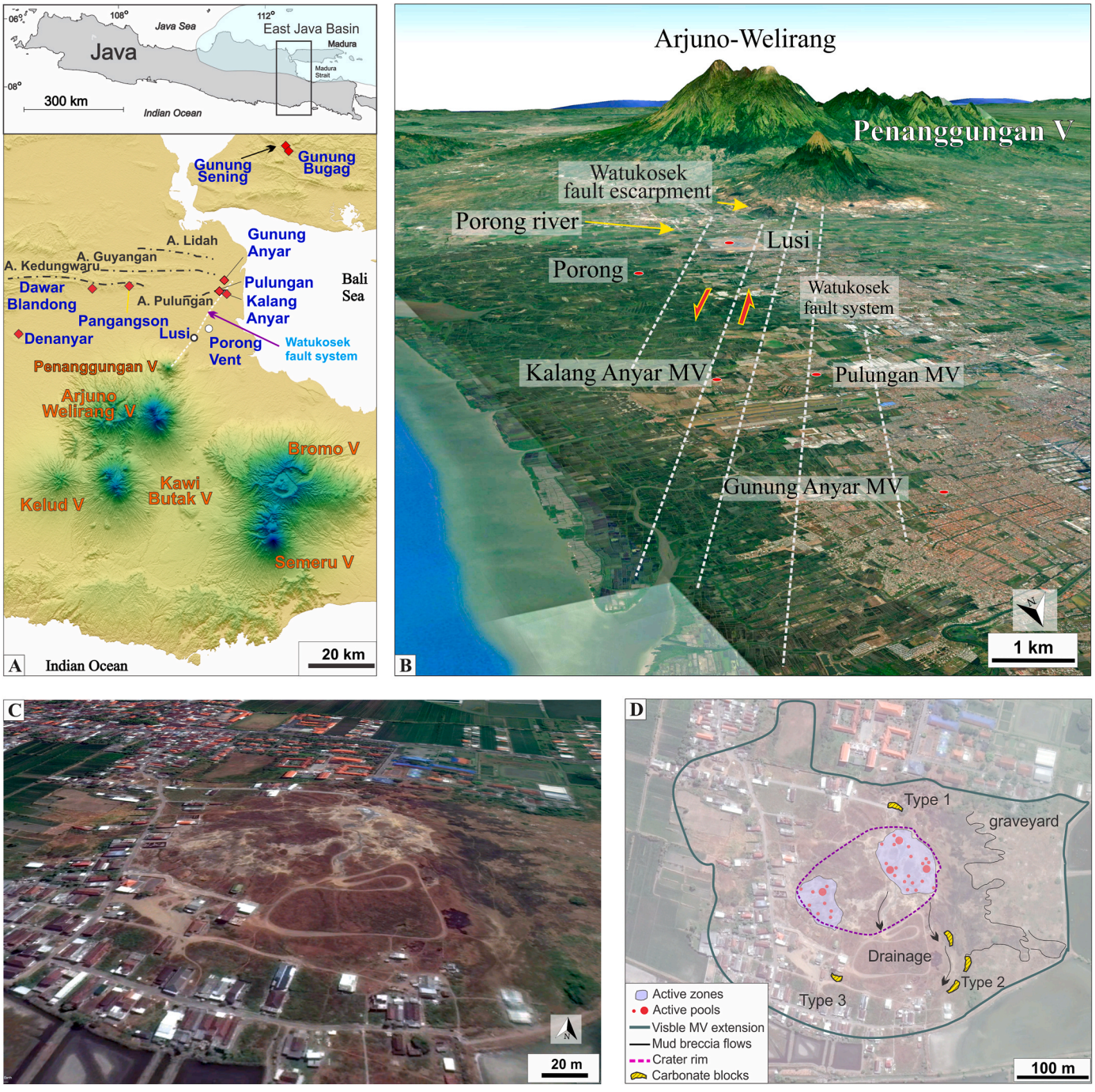

Fig. 1. North-east Java Island and Kalang Anyar MV. (A) Elevation map showing the main structures of the volcanic arc (to the south) and in the sedimentary basin (to the north). Inset map of Java Island with a portion of the East Java basin indicated (light blue shading). (B) Google Earth satellite image with the position of the main piercements and tectonic structures. (C) Google Earth satellite image showing a pie-shaped morphology. Note lighter coloured areas characterized by more intense fluids emissions, and darker regions poor of vegetation where salt enriched mud breccia flows are deposited. (D) Main features of Kalang Anyar MV superimposed on a Google Earth satellite image. The crater zone contains two main active seepage regions with numerous pools release gas, water and mud (red dots). Carbonate chemoherm blocks are present on the outskirts of the crater zone. The extension of the MV (green framing line) is approximate due to the presence of cultivated fields and constructions. (For interpretation of the references to colour in this figure legend, the reader is referred to the Web version of this article.)

at the surface in particular along the Watukosek escarpment (a fault escarpment adjacent the Penanggungan volcano of the Arjuno-Welirang volcanic complex), the sharp bent path of the Porong River, and the numerous sinistral strike slip faulted/fractured zones (including a well developed system of antithetic fracture zone) observed in a vast region around the Lusi eruption. Several piercements have been identified along the WFS: Lusi (the largest active sediment-hosted hydrothermal system-SHHS), the Porong palaeo-vent, and the Kalang Anyar, Gunung Anyar, and Pulungan mud volcanoes (Mazzini et al., 2012; Lupi et al., 2013; Miller and Mazzini, 2018). Several authors have presented evidence that the WFS promotes the rise of mantle-derived fluids in the southernmost part of the basin (Mazzini et al., 2012; Inguaggiato et al., 2018; Sciarra et al., 2018; Zaputlyaeva et al., 2019). However, no targeted geochemical studies have tackled the migration of mantle-derived fluids into the back-arc sedimentary basin. Hence it remains unclear how far north the influence of the WFS extends in terms of assisting the migration of deep fluids. Investigations of MVs have been only recently introduced in Indonesia and many open questions persist regarding their plumbing systems and duration of activity.

Worldwide, mud volcanoes have been investigated using geochemical (e.g. Mazzini and Etiope, 2017 and refs therein), geological (e.g. Akhmanov et al., 2003) and numerical (Collignon et al., 2018 and refs therein) methods. As yet, relatively few geophysical experiments have targeted onshore mud volcanoes and their associated signals. Seismic experiments have been conducted at the Dashgil, Azerbaijan (Albarello et al., 2012) Santa Barbara (Gattuso et al., 2021) and Nirano Mud Volcano, Italy (Lupi et al., 2016; Antunes et al., 2022), and a similar approach has been applied to the Lusi mud eruptive system (Karyono et al., 2017). These settings have been further investigated with geoelectrical methods (Lupi et al., 2016; Mazzini et al., 2021b), gravimetric data (Mauri et al., 2018a, 2018b; Osorio Riffo et al., 2021) and UAV surveying (Di Felice et al., 2018; Di Stefano et al., 2018). Further, the study of MVism typically focuses either on onshore or offshore structures. So far there is paucity of dedicated studies on MVs that display progressive evolution from subaqueous to subaerial conditions.

The objective of this study is to present a multidisciplinary study of Kalang Anyar MV, based on geological and geophysical field surveys and geochemical analyses of samples. The results provide evidence of deep gas sources in relation to tectonic structures, on the mud volcano plumbing system, and on the recent history of extrusion and its geohazard potential. To our knowledge, this is the first survey of an Indonesian mud volcano that aims to quantify its gas emissions and compare them with similar structures elsewhere on the planet. It is also the first study of a mud volcano that records a progression from submarine to terrestrial activity.

2. Geological setting

The East Java sedimentary basin (Fig. 1A) is a petroleum-rich region that broadly extends in the Java Sea and includes the north-eastern part of Java Island (Satyana and Darwis, 2001; Doust and Noble, 2008 and refs. therein). The basin is bound to the south by an east-west oriented volcanic arc (Fig. 1A). The study area is located in the north-east back-arc of Java Island (Fig. 1A and B). The stratigraphy of this southern part of the basin is constrained by seismic data correlated to drilling results and includes sequences of Plio-Pleistocene shales and volcaniclastic deposits (Upper Kalibeng Fm), capping Miocene marls (Tubang Fm), Miocene-Oligocene carbonates (Kujun Fm) and Eocene shales represented by the regional Ngimbang Fm. source rock (i.e. Mudjiono and Pireno, 2002; Satyana and Purwaningsih, 2003; Miller and Mazzini, 2018; Moscariello et al., 2018). Three MVs are located ~40 km towards the NE of the Arjuno-Welirang volcanic complex along the Watukosek Fault System (WFS) (Fig. 1). This fault system originated from the Arjuno-Welirang volcanic complex, extends towards the north east of the island and it has been identified on the seismic data and at the surface (e.g. Moscariello et al., 2018; Obermann et al., 2018; Sciarra et al., 2018; Zaputlyaeva et al., 2019; Mazzini et al., 2021c; Manton et al., 2022). Pulungan and Kalang Anyar MVs lie along the Pulungan anticline while Gunung Anyar (meaning "New Mountain") MV is located along of the Guyangan anticline. Kalang Anyar is located 2.7 km south of the Surabaya Juanda Airport (Fig. 1A and B). These anticlines manifest at the surface as morphological highs and are the result of the subduction-related compressional regime that has characterized the island since middle Miocene (e.g. Satyana et al., 2004; Hall et al., 2007; Clements et al., 2009; Novianto et al., 2020).

3. Methods

Kalang Anyar was visited during four field expeditions in 2006, 2008, 2012, and 2016 and investigated using a multidisciplinary approach involving analyses of satellite imagery, geochemical analyses, gas flux measurements and seismic monitoring. Google Earth satellite imagery from 2002 have been used to compare the gradually increasing construction of settlements inside the MV area. Recent satellite images have been used to examine the morphology, mud flow patterns and to identify and quantify the active seepage sites within the crater.

3.1. Geochemistry

3.1.1. Gas analyses

Gas samples from bubbling seeps were collected using an inverted plastic funnel connected by silicone/Tygon® tubes to pre-evacuated 100 mL glass flasks. At each site, three different samples were obtained. Analyses of molecular and isotopic gas composition were completed at the Institute for Energy Technology (IFE), Norway, using a Hewlett Packard 5890 Series II GC equipped with a Porabond Q column, coupled with a flame ionisation detector (FID), a thermal conductivity detector (TCD) and a methylization unit (see more details in Mazzini et al., 2012). The 2016 samples were analysed in the laboratories of INGV (Istituto Nazionale di Geofisica e Vulcanologia) of Rome and Palermo (Italy) for the determination of the molecular and isotopic composition of CO_2 and CH_4, respectively. Molecular composition was analysed using a MicroGC Varian 4900 CP, equipped with two Thermal Conductivity Detectors (capillary columns: 10 m PoraPLOT U and 20 m Molsieve 5 A), with an error of ±3%. Carbon and hydrogen isotopes of methane were carried out on a Delta Plus XP CF-IRMS instrument (Thermo, Bremen, Germany) coupled with a TRACE GC equipped with a Poraplot-Q capillary column (30 m _ 0.32 mm i. d.) and using a flux of 0.8 cc min^{-1} of pure helium (5.6 grade) as gas carrier. GC III combustion interface was used to produce carbon dioxide from methane. GC-TC interface provides on-line high-temperature methane conversion into hydrogen suitable for isotope analyses. Typical reproducibility for measurements of $\delta^{13}C$ (1s = 0.1‰) and $\delta D\text{-}_{CH4}$ (1σ = 1‰) is better than 0.2‰ and 2.5‰ respectively.

At one site with sustained gas seepage, a sample for He analyses was collected in annealed copper tubes sealed directly in the field using a cold welding clamp. The sample was analysed at the INGV laboratory in Palermo. After standard purification procedures, ^3He, ^4He and ^{20}Ne, and the $^4He/^{20}Ne$ ratios were determined by separately injecting He and Ne into a split flight tube mass spectrometer (GVI-Helix SFT, for He analysis) and then into a multicollector mass spectrometer (Thermo-Helix MC plus, for Ne analysis). The analytical error was generally less than 1%. The R/R_A values were corrected for atmospheric contamination based on the $^4He/^{20}Ne$ ratio (Sano and Wakita, 1988). The results are given in R/Ra notation, where R is the sample $^3He/^4He$ ratio and Ra is the atmospheric $^3He/^4He$ ratio, 1.39×10^{-6}. The Ar-isotope composition was measured in a multicollector mass spectrometer (GVI Argus), for which the analytical uncertainty was 0.5%. The new gas analyses are integrated with data documented in Mazzini et al. (2012).

3.1.2. Carbonate analyses

Carbon and oxygen stable isotopic analyses were undertaken at the

Institute for Energy Technology (IFE, Norway) on both a) bivalve shells associated to the carbonate blocks and b) carbonate cements from different outcrops inside the MV crater. The carbonate cements were ground and digested with a 0.1 mL 100% H_3PO_4 solution for 2 h at 30.0 °C in a vacuumed environment. The released CO_2 was transferred to a Finnigan MAT DeltaXP isotope ratio mass spectrometer (IRMS), for determination of $\delta^{13}C$ and $\delta^{18}O$. The analyses were controlled by in-house standards of calcite and aragonite. Results are reported in ‰ relative to the V-PDB standard. The precision for $\delta^{13}C$ is ±0.1‰ and for $\delta^{18}O$ ± 0.2‰.

3.1.3. Radiocarbon measurements

Radiocarbon (^{14}C) measurements were made on two types of bivalve shells associated with carbonate blocks: a) clam shells cemented within the carbonate blocks from the north-east of the MV structure (sample JV08-02 S) and b) oyster shells present on the external surfaces of carbonate blocks from the southeast of the MV structure (sample JV08-03 S). An initial attempt was made to measure the calendar age of the carbonate blocks themselves using U–Th dating. Unfortunately, the carbonate cements were an open system with respect to U, making it impossible to obtain reliable results (D. Sahay, pers. comm.). To obtain a reliable age of deposition using the radiocarbon method requires measuring carbon that represents the contemporaneous atmospheric CO_2 at the point of deposition (i.e., excluding carbon of geological origin). For this reason, shells were selected for dating, as having the greatest likelihood of meeting these criteria.

Shells were selected for analysis on the basis of stable isotopic results (see Table 1) and prepared in the NEIF Radiocarbon Laboratory at the Scottish Universities Environmental Research center (SUERC). The sample treatment included etching to remove 20% of the dry weight of material by controlled hydrolysis with dilute (0.5 M) HCl. The CO_2 evolved from the etching process was purged from the hydrolysis vessel with N_2 gas and the etched sample was then hydrolysed to CO_2 using 2 M HCl. An aliquot of this CO_2 was used for off-line $\delta^{13}C$ determination by Isotope Ratio Mass Spectrometry, for normalizing ^{14}C results. The sampled CO_2 was converted to graphite by Fe/Zn reduction for subsequent ^{14}C measurement by Accelerator Mass Spectrometry (AMS).

The measured ^{14}C ages were converted to calendar age ranges using OxCal v4.4 and the Marine20 calibration curve (Ramsey, 1995; Reimer et al., 2020), together with a Delta R (ΔR) value for the Java region of −90 ± 49. This ΔR was obtained from a weighted mean of values from Sabui Bay, South Borneo, and Pelabuhanratu, Java as reported in Southon et al. (2002). These ΔR values are the closest spatially available to Kalang Anyar and are internally consistent on the basis of a chi-squared test (c.f. Ward and Wilson, 1978). The ΔR values reported in Southon et al. (2002) were recalculated using SHCal20 (Hogg et al., 2020) before being combined. Java is in a zone where a mixed north and south hemisphere ^{14}C calibration curve is recommended, due to monsoon-driven variability in the ITCZ (Hogg et al., 2020). However, calculating values with INTCAL20 shifted the ΔR values by an amount that is insignificant with respect to the uncertainties on the measurement, so the decision was taken to use the SHCal20-derived values.

3.2. CO_2 and CH_4 flux measurements

We completed 27 CH_4 and CO_2 flux measurements crossing the MV along the A-A' profile using the West Systems™ portable fluxmeter equipped with CO_2 and CH_4 detectors. The CH_4 flux meter is a TLD Tunable Laser Diode spectrometer (West Systems™) that allows the measurement of gas fluxes in the range from 1.5 up to 1000 mol $m^{-2}d^{-1}$. The CO_2 detector is a LICOR–LI820, which is very accurate from 1.5 up to 300 mol $m^{-2}d^{-1}$. The acquired data were statistically and graphically processed with the Statistica 10 and Grapher 18 software. The total CO_2 and CH_4 soil release was estimated from the measured flux values following the approach described by Chiodini and Frondini (2001).

3.3. Seismic signal monitoring

To identify seismic signals potentially associated to bubbling observed at the main seepage sites, we deployed 4 broadband seismometers (three 120s Trillium compact and one Leinartz 3Dlite equipped with Nanometrics Taurus digitizers) for 24 h. The differences in seismic signals were found to be drastically different between day and night. This is due to day-time human activity in the study area. For instance, the shoulders of the mud volcano have small tracks that are record the passing of scooters and motorcycles. To minimize anthropogenic noise, we only inspected night-time seismic data and discarded the day-time records.

4. Results

4.1. Morphology and surface observations

Kalang Anyar MV has an overall smooth pie morphology that extends over a surface of ~1.5 km^2 reaching a relative maximum elevation of ~7 m in some areas of the crater site. The exact extension of the mud breccia flows cannot be defined precisely since the surroundings of the structure are either occupied by cultivated fields or by constructions. The elevated crater zone (~0.5 km^2) is rimmed by a steeper ~2 m tall ring wall and gently dips on its southern side (Fig. 1C). Two distinct areas of the crater are characterized by active seepage of gas, mud, and water at dozens of bubbling pools (Fig. 1C and D, Fig. 2). Active pools varied in their sizes (ranging from few centimetres up to 2 m in diameter) and degassing intensity (Fig. 2A–F). These sites are uniformly surrounded by salt crusts, consistent with the seepage of elements-enriched waters. Some of the pools are surrounded by thriving microbial colonies displaying different colours (greenish, yellowish, brownish) and thicknesses (Fig. 2C and D). Thicker salt crusts may be observed inside some of the pools where the elevated evaporation and the lack of rain during the dry season gradually increases the salinity levels (Fig. 2E). Some of the pools also display traces of active oil seepage (Fig. 2F).

4.2. Carbonate blocks

Three different types of carbonate blocks are observed at multiple localities in the outer part of the crater (Fig. 1D). Type 1 is present in the

Table 1
Isotope analyses of carbonate samples. For carbonate blocks and ridges location refer to map in Fig. 1D.

Station number		$\delta^{13}C$ (‰ V-PDB)	$\delta^{18}O$ (‰ V-PDB)	^{14}C Enrichment (% Modern±1 σ)	Age ^{14}C years BP ± 1 σ	Comments
JV08-02	Type 1	−44.4	−3.3	-	-	Porous carbonate cement (NE)
JV08-02 S	Type 1	−12.2	−4.6	0.37 ± 0.06	44,917 ± 1306	Shell (bivalve clams) (NE)
JV08-03	Type 2	−37.1	−1.3	-	-	Carbonate cement (SE)
JV08-03 S	Type 2	−3.1	−6.2	76.35 ± 0.35	2167 ± 37	Oyster shell (SE)
JV12-03	Type 2	−48.8	0.7	-	-	Carbonate cement (SE)
JV12-01	Type 2	−38.2	0.1	-	-	Carbonate cement (SW)

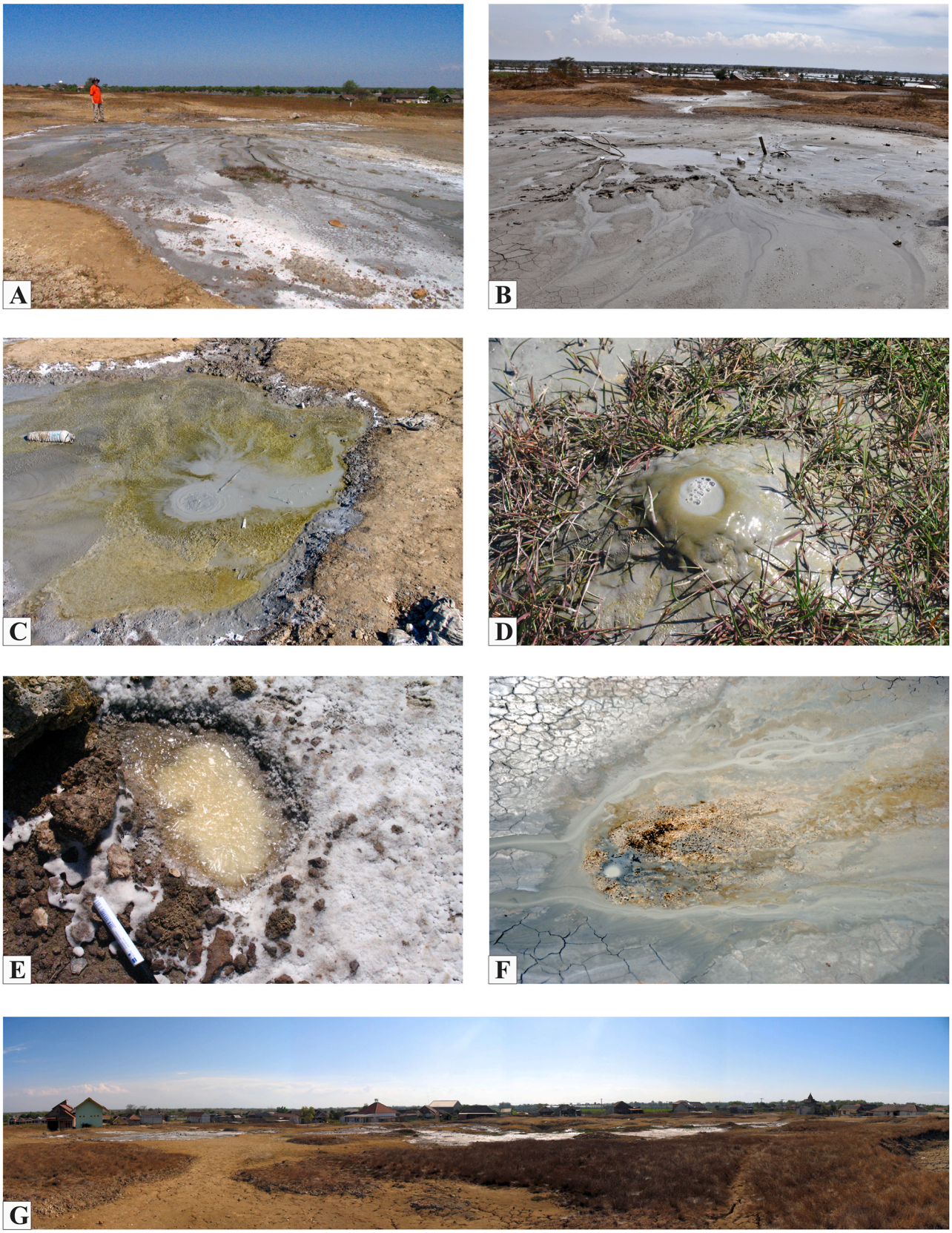

Fig. 2. Seepage sites at Kalang Anyar MV. (A–B) examples of some of the larger active pools with salt crusts surrounding areas where a radial discharge of water continuously takes place; (C–D) thriving microbial colonies of differing colours and textures; (E) example of a salt crust in and around pools; (F) example of oil films at seepage sites; (G) panorama of one side of the MV showing the numerous seeps and, in the background, constructions inside the crater zone. (For interpretation of the references to colour in this figure legend, the reader is referred to the Web version of this article.)

Fig. 3. Various types of methanogenic carbonates at Kalang Anyar MV. (A–B) Type 1: chemoherms blocks with chemosymbiotic bivalves. (C–D) Type 2: elongated carbonate ridges coated on their external surface by centimetre- (C) and decimetre-sized (D) oysters. (E) Type 3: large massive carbonate with cemented shells. (F) Shell debris on the surface of the crater zone.

NE part of the structure and is densely packed with bivalves (chemoherms) (Fig. 3A and B). Type 2 crops out at several localities in the southern part, either as isolated meter-sized blocks or forming elongated ridges (Fig. 3C and D), and consists of more massive carbonates covered on their external surface by oyster shells ranging in size from centimetres to decimetres. Type 3 is present in the south-western part of the MV consisting of massive carbonate with cemented shells. The results of carbon and oxygen stable isotope analyses from Types 1 and 2 are presented in Table 1. The shells gave $\delta^{13}C$ values between −12.2 and −3.1‰ and $\delta^{18}O$ values between −6.2 and −4.6‰ (Fig. 4). The bulk carbonate samples have $\delta^{13}C$ and $\delta^{18}O$ values in the range of −48.8 to −37.1‰ and −3.3 to 0.71‰.

Radiocarbon (^{14}C) measurements (Table 1) were performed on shells to constrain the time period during which these organisms were living. The bivalve clams collected from carbonate blocks Type 1 (JV08-02 S) returned a measured ^{14}C age of 44,917 ± 1306 BP. As this age is

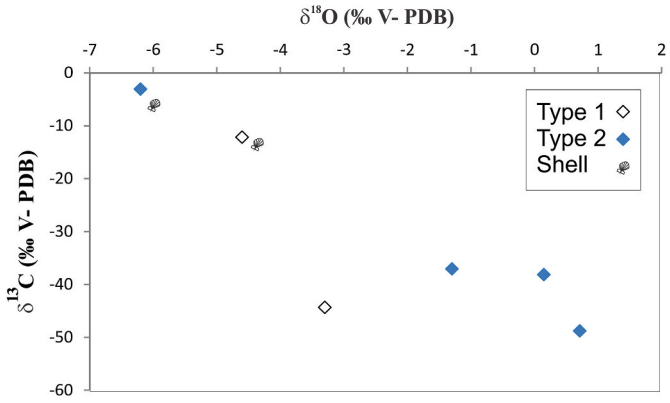

Fig. 4. Carbon and oxygen isotope values for the carbonates Types 1 and 2 outcropping at different localities in the crater outskirts of Kalang Anyar MV.

inconsistent with submarine conditions in the study area (see discussion), we did not proceed with calibration of the measured age (see section 5.2). For oyster shells cemented outside the carbonate blocks Type 2 (sample JV08-03 S) the measured ^{14}C age was 2167 ± 37 BP. The calibrated calendar age range for this sample at 2 sigma (95.4% confidence) is 1890-1488 BP.

Abundant shell debris, corals, and occasional fish teeth (Fig. 3F) are scattered across the surface of the mud volcano. This type of debris appears to be present only on the surface. The sediments forming Kalang Anyar MV consist of mud breccia, a mixture of clayey-silty-sandy matrix that incorporates larger clasts of different lithologies (mudstone, sandstone, carbonates) and size from centimetric and up to 15 cm. The presence of mud breccia is typical for most MVs worldwide (e.g. Mazzini and Etiope, 2017 and refs. therein) and provides insights into the stratigraphy pierced by the MV conduit.

4.3. Gas geochemistry

Results of gas sampling show that the sampled seepage sites are CH_4-dominated (89% < CH_4 < 96%) with smaller amounts of CO_2 (up to 10.5%) and minor contents of ethane and propane (Table 2). Measured $\delta^{13}C_{CH4}$ values range between −48.4 and −55.7‰, values of δD_{CH4} between −214 and −219‰, and $\delta^{13}C_{CO2}$ between −6.6 and −10.5‰. He isotopic analyses of gas samples revealed $R/R_A = 0.5$, $^4He/^{20}Ne = 1.4$ and $^{40}Ar/^{36}Ar = 305.0$ (Table 3).

4.4. Gas fluxes

Etiope (2015) provides a summary of the natural gas seepage modes and classifies these as: a) macro-seepage where focused gas emissions occur (e.g. either dry seeps, a crater, a vent, or a flame; oil seeps; or a bubbling pool, a salsa lake, a gryphon typically present at mud volcanoes); b) miniseepage defining the invisible, diffuse exhalation of gas surrounding visible seeps within a macro-seepage zone (i.e. a sort of halo that surrounds a focused seep) and a transition area exists where gas emissions gradually decreases furthering away from the macro-seepage sites after tens or hundreds of meters; c) microseepage as pervasive, diffuse exhalation of gas from soil, independent of the presence of macro-seeps. The last mode typically occurs in gas-oil-prone sedimentary basins.

Gas flux measurements along the A-A' profile (Fig. 5A and B) revealed φCH_4 rates ranging from 0.0005 to 643 g m^{-2} d^{-1} with mean rates of 64 g m^{-2} d^{-1}, while φCO_2 ranged from 1.18 to 180 g m^{-2} d^{-1} (mean rates 38 g m^{-2} d^{-1}, Table 4).

Two gas exhalation modes are identified in the study area: a) diffuse invisible seepage, characteristic for the whole area covered by mud breccia (miniseepage) and b) active seeps in the crater zone, where gas is intermittently or continuously expelled together with water and mud (macro-seepage). Results along the profile indicate that gas exhalation occurs at different strengths at two main regions within the MV (Fig. 5A and B, Table 5). The *crater zone* is characterized by macro-seepage (φCH_4 between 8.03 and 643.36 g m^{-2} d^{-1} and φCO_2 between 53 and 180 g m^{-2} d^{-1}) and miniseepage modes (φCH_4 between 0.02 and 0.095 g m^{-2} d^{-1} and φCO_2 between 7.82 and 34.81 g m^{-2} d^{-1}), while the *surrounding region* is characterized by miniseepage only (φCH_4 between 0.0005 and 0.027 g m^{-2} d^{-1} and φCO_2 between 1.18 and 49.06 g m^{-2} d^{-1}) at significantly lower rates. For this reason we decided to treat these two regions separately and calculate separate budgets for gas emissions (Table 5).

The total output of macro-seeps measured in the active crater zone (Fig. 1D) yields an emission rate of 2.50 and 0.85 kg d^{-1} for CH_4 and CO_2, respectively (Table 5), with a mean emission value of 0.09 kg d^{-1} and 0.28 kg d^{-1} (for CO_2 and CH_4, respectively). These values were applied to the number of active macro-seeps identified in situ, but not measured, that were digitalised from satellite images. Using this approach, we estimated a gas emission from macro-seeps of 13.31 kg d^{-1} for CH_4 and 4.44 kg d^{-1} for CO_2, or 1.62 and 4.86 t yr^{-1} for CO_2 and CH_4, respectively (Table 5). Statistical analyses of the whole dataset of fluxes (macro-, miniseepage areas) show that CO_2 is much less dispersed than CH_4 (standard deviation of 41 g m^{-2} d^{-1} vs 152 g m^{-2} d^{-1} respectively, Table 4). The scatter plot of φCH_4 vs φCO_2 (Fig. 5C) shows that a good correlation is present only on the measured macro-seeps (r = 0.9).

Using the Chiodini and Frondini (2001) approach we calculated a mean miniseepage rate from the measurements in the crater zone and applied it to the mapped crater surface (0.0197 km^2). The calculation reveal a CH_4 flux rate of 5.22 t yr^{-1}. Similarly, CH_4 miniseepage rate was estimated for the area surrounding the crater zone (0.14 km^2) using the average measured values (0.01 g $m^{-2}day^{-1}$) to obtain an estimated flux of 0.54 t yr^{-1}. Concerning CO_2 miniseepage rates: the flux

Table 2
Molecular composition of sampled gasses in vol. %. Bdl: below detection limit; nd: not determined.

Station number	Locality	Comments	T int. °C	C1	C2	C3	iC4	nC4	He	H_2	CO_2
JV06-12	Kalang Anyar	Small seep outside main dam with microbial colonies around	30.6	95.542	0.106	0.001	0.006	bdl	nd	nd	4.344
JV06-13	Kalang Anyar	Small seep	31.2	96.793	0.115	0.001	bdl	bdl	nd	nd	3.091
JV06-16	Kalang Anyar	Small seep	32.9	90.538	0.114	0.010	bdl	bdl	nd	nd	9.338
JV08-02	Kalang Anyar	Large field of several pools where mainly water and gas seep out	31.0	96.034	0.111	0.009	0.001	0.001	nd	nd	3.845
JV16-04	Kalang Anyar	5–10 cm seep bubbling with microbial mats around	32.2	91.328	0.040	<0.005	bdl	bdl	0.011	0.007	8.614
JV16-05	Kalang Anyar	Small Salsa lake (3 × 4 m in size) formed by numerous seeps (~30) expelling watery mud. Warmer fluids expelled.	36.4	89.380	0.140	<0.005	bdl	bdl	0.012	0.009	10.459

Table 3
Isotopic composition of sampled gasses. Isotopic data: $\delta^{13}C$: ‰, VPDB; δD: ‰, VSMOW; atm. R/Ra = ($^3He/^4He$) sample/($^3He/^4He$) atmosphere; Ra = 1.39×10^{-6}; nd: not determined.

Station number	Locality	$\delta^{13}C_1$ (‰ V-PDB)	δD_1 (‰ V-SMOW)	$\delta^{13}C_{CO2}$ (‰ V-PDB)	R/Ra	Rc/Ra	$^4He/^{20}He$
JV06-12	Kalang Anyar	−55.0	−214	−9.9	nd	nd	nd
JV06-13	Kalang Anyar	−55.7	−214	−6.1	nd	nd	nd
JV06-16	Kalang Anyar	−55.0	−216	−4.0	nd	nd	nd
JV08-02	Kalang Anyar	−48.4	−219	−16.5	nd	nd	nd
JV16-04	Kalang Anyar	−55.1	−215	−6.6	nd	nd	nd
JV16-05	Kalang Anyar	−48.9	−216	−10.5	0.34	1.4	305.0

measurements, with the exception of a few localities in the eastern sector, revealed values below 20 g m^{-2} day^{-1}. This value is commonly considered as the threshold to define background emissions in the range of typical vegetative soil respiration (e.g. Baldocchi and Meyers, 1991; Norman et al., 1992). Therefore, CO_2 miniseepage was not considered in the final calculation for the budget of geo-gas emitted from Kalang Anyar MV. The total combined gas emission rates for CO_2 and CH_4 over the whole MV surface are estimated to be 1.62 and 5.75 t yr^{-1}, respectively (Table 5).

4.5. Seismic signals

High-frequency tremors were recorded at all 4 seismometers deployed around the MV crater (Fig. 5A). Fig. 6 shows an example of the emergent signals (lasting on average 100 s) that characterize Kalang Anyar. The signal is clearly recognizable on all three components of each of the 4 seismic sensors. The waveforms are similar to those recorded at other active mud volcaniclastic systems and referred to as drumbeats (e.g. Lupi et al., 2016; Karyono et al., 2017). The amplitude of the waveforms rapidly decays away from the main seepage sites and reaches first the northernmost station (i.e. KALB2, that is the closest one to the bubbling vents). Such a rapid decay, previously described by Karyono et al. (2017) at the Lusi eruption site, may be explained by the high-frequency content of the signal (most prominent between 8 Hz and 12 Hz – Fig. 6b). Lupi et al. (2018) used a cross-correlation method (fully described by Minetto et al., 2020) to locate this emergent signal and showed that the highest probabilistic occurrence of the source falls close to the active vent region.

5. Discussion

Our multidisciplinary study provides numerous insights into the dynamics and the history of Kalang Anyar MV. In particular, the integration of geological, geophysical and geochemical surveying sheds light on large scale fluid migration through the plumbing system both at depth and near the surface, and on sedimentary processes during the transition from marine to terrestrial mud volcanic activity.

5.1. Authigenic carbonates and submarine seepage activity

The formation of methanogenic carbonates has been documented at numerous submarine seepage sites worldwide, including cold seeps, pockmarks, pingos, and seep mounds (Hovland and Judd, 1988; Michaelis et al., 2002; Mazzini et al., 2006; Ivanov et al., 2010; Judd et al., 2020). These precipitates are by-products of anaerobic oxidation of methane mediated by consortia of anaerobic methanotrophic (ANME) and sulphate reducing bacteria (SRB) that live in symbiosis at seepage sites (e.g. Boetius et al., 2000; Valentine and Reeburgh, 2000; Boetius and Wenzhofer, 2013). Seep carbonates (or authigenic carbonates) are characterized by negative $\delta^{13}C$ isotopic values confirming that microbial oxidation of hydrocarbons (typically methane) was the source of dissolved inorganic carbon in the pore solutions. Submarine MVs, where methane seepage is or has been active, are typically associated with carbonate deposits that vary in form and extent depending on the modality of fluid release (e.g. Aloisi et al., 2000; Mazzini et al., 2004; Mazzini et al., 2008; Dupré et al., 2010; Magalhães et al., 2012; Vanneste et al., 2012; Pierre et al., 2014). Seepage sites represent oases where microbial colonies, chemosymbiotic species and opportunistic fauna thrive in communities (Sibuet and Olu, 1998; Cordes et al., 2009, 2010; Vanreusel et al., 2009; Campbell et al., 2010; Ritt et al., 2011; Cunha et al., 2013; Hatem et al., 2014; Levin et al., 2016).

The cements of authigenic carbonate blocks and ridges sampled at Kalang Anyar MV (Table 1) have $\delta^{13}C$ isotopic values that are typical of methanogenic carbonates, indicating that submarine methane seepage and carbonate precipitation was ongoing at this locality. $\delta^{13}C$ isotopic values ranging between −37.1 and −48.8‰ suggest the seepage of a mixed microbial-thermogenic methane, which is in agreement with isotopic analyses of currently seeping gas at the crater site (Tables 2–3). Similar to many other seepage sites, the Kalang Anyar carbonates are associated with bivalves (clams and oyster) that also reveal negative $\delta^{13}C$ values (Fig. 4). Clams (Type 1, $\delta^{13}C$ = -12.2‰) are cemented within the methanogenic carbonate and during their growth, also incorporated some ^{13}C depleted C originating from the oxidation of methane, while oysters (Type 2, $\delta^{13}C$ = -3.1‰) are observed exclusively on the outer part of the blocks and therefore are less affected by ^{13}C depleted C. Recent subaqueous conditions at Kalang Anyar MV are further supported by the shell debris scattered across the surface of the mud volcano (Fig. 3F).

5.2. Timing of submarine seepage relative to sea level changes

Radiocarbon (^{14}C) results from bivalve shells that were living during the precipitation of methanogenic carbonates are best candidates to constrain the age of submarine methane seepage. When dating the bivalves, it is important that the $^{14}C/^{12}C$ of the shells (from which the % Modern C and ^{14}C age are calculated) represents the dissolved inorganic carbon (DIC) of the seawater at the time the shell was precipitated. In the setting of Kalang Anyar MV, two potential carbon sources can be identified. First, the DIC of the ocean water for the region, which best represents the 'true' ^{14}C age (and calendar age, following calibration) at the time the shell was living. Second, DIC from geological sources (e.g. from the seepage of methane), which is older and likely to be^{14}C-dead' at source. The measured $^{14}C/^{12}C$ ratio (and hence radiocarbon age) of the shells is a weighted average of these two possible end members. The greater the contribution of geological carbon (through localized methane seepage), the greater will be the 'apparent' ^{14}C age of the sample. In principle it is possible to correct for the geological contribution through an isotope mass-balance approach using a system such as $\delta^{13}C$ and/or $\delta^{18}O$. However, this requires an accurate assessment of the end member values and the uncertainty associated with these. We chose not to attempt correction for the incorporation of geological carbon and instead use the ages of the samples to constrain the chronology of events in a general sense, providing only maximum ages.

The ^{14}C results for sample JV08-02 S show a value of 0.37 ± 0.06 % MC which translates to a^{14}C age of ~45 Ka BP (see Table 1). This age is inconsistent with regional evidence that at this time sea level in the study area was 40–120 m lower than today (Van den Bergh et al., 1996 and refs therein). In addition, our carbon isotopic results indicate the incorporation of small amounts of geological (^{14}C dead) carbon within the shells, which are cemented within carbonate blocks that have

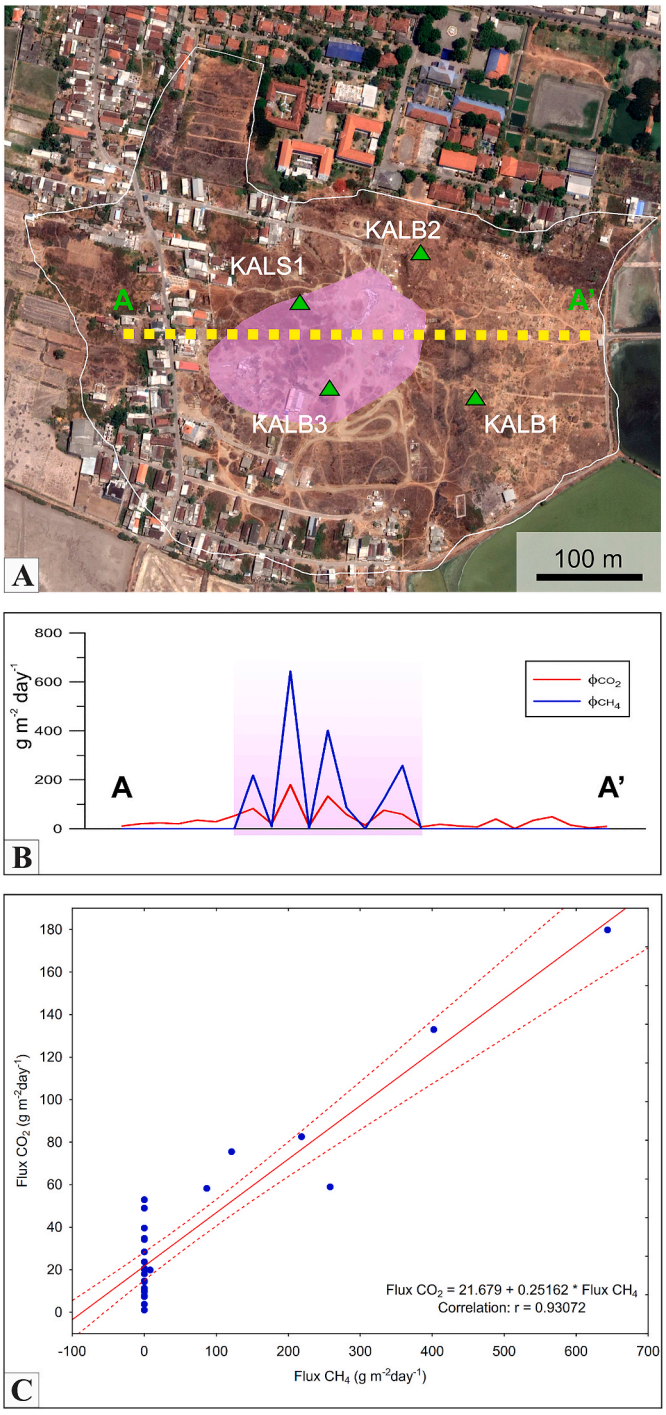

Fig. 5. Summary of CH_4 and CO_2 flux measurements along a profile across Kalang Anyar MV. (A) Google Earth satellite image showing the flux profile A-A′, the positions of the four seismometers (green triangles marked KALB1-KALB2-KALB3-KALS1), the extension of Kalang Anyar MV (white line), the crater zone (purple shaded area). (B) Plot of flux along line A-A' (at top) showing significant increase of both CH_4 and CO_2 emissions in the crater area. (C) Scatter plot of φCH_4 vs φCO_2 shows a strong positive linear relationship highlighted by the trend line that marks the best fit on the measured macro-seeps. (For interpretation of the references to colour in this figure legend, the reader is referred to the Web version of this article.)

negative $\delta^{13}C$ values (see Table 1). We hypothesise that through diagenetic processes the ^{13}C-depleted methanogenic cement is incorporated in the bivalve shells (although this is not strongly revealed by the isotope analyses). We cannot currently solve this issue without a wider programme of investigation, and, in light of this uncertainty, we decided not to consider the ^{14}C analytical results for sample JV08-02 S in our interpretation of the timing of activity at the study site.

The result for sample JV08-03 S is 76.35 ± 0.35% MC (Table 1), corresponding to a ^{14}C age of ~2 Ka BP (calibrated age range at 95% 2310-2006 BP). These oysters bivalve were sampled from the external surface of the blocks and have $\delta^{13}C$ values close to zero. Therefore, these represent the best candidate to provide an upper (most recent) calendar age for methane degassing. Nonetheless, due to the possible incorporation of geological carbon, this is considered a maximum age for the sample. However, the young age relative to that for JV08-02 S, coupled with stable isotope results, indicates that the proportion of geological carbon that may form part of the total sample carbon is low.

Kalang Anyar MV currently lies ~5 km from the shore of the Java Sea. This region is essentially flat with very gentle slopes and reaches a maximum elevation of ~2 m in the area around the MV. Methanogenic carbonates are abundant on the southern part of the structure where the ground elevation is ~2 m. Mann et al. (2019) assembled a database of Holocene relative sea-level changes for the broader south and southeast Asian region including part of the Java Sea where Kalang Anyar MV is located. The authors show that relative sea level in this region was a few meters higher between 3 and 8 thousand years ago, and has been progressively dropping since ~8 Ka. This sea level drop during the past several thousand years is typical for equatorial regions and is caused by a process that Mitrovica and Peltier (1991) termed "equatorial ocean siphoning", which results from the solid Earth's viscous response to ice age deglaciation. Isostatic adjustment to the loss of ice sheet mass in North America, Eurasia, and Antarctica caused the collapse of peripheral bulges around these ice sheets. This subsidence generally depressed the seafloor, which expanded the volume of the ocean basins and lowered sea level in the equatorial regions far from the former ice sheets (Mitrovica and Milne, 2002).

Our shell age for sample JV08-03 S (~2 Ka BP) is also consistent with the broad sea level changes expected for the SE Asia and suggest that the coastal region to the south of Surabaya was also submerged at this time. We further suggest that the elevation of the studied region has been increasing during the last few thousands years. Evidence supporting this is related to two factors. The first is associated to the current Neogene compressional regime ongoing in the back-arc of the island (Satyana et al., 2004; Clements et al., 2009; Novianto et al., 2020) as also highlighted by GPS monitoring that record an overall gentle uplift in the region (Gunawan and Widiyantoro, 2019). The second factor is related to the gradual elevation increase that is commonly observed vbgat MVs (like Kalang Anyar) that are characterized by frequent eruptions (e.g. Mazzini and Etiope, 2017). Considering that the erupted mud breccia is easily erodible and that significant amounts of sediments are transported during the rainy seasons, we suggest that previous eruptions must have expelled significant volumes of sediment.

To our knowledge Kalang Anyar MV represents the first example of currently active onshore sedimentary volcanism displaying deposits of methanogenic carbonates and revealing evidence of previous subaqueous eruptions and methane degassing.

5.3. *Insights into fluid sources from oxygen stable isotope geochemistry*

Oxygen stable isotope analyses of carbonate cements are a powerful tool to estimate fluid compositions and/or the equilibrium temperatures at which carbonate cements precipitate (e.g. Naehr et al., 2007 and refs therein). Typically, ^{18}O enrichment is equivalent to colder precipitation temperatures. When isotopes reveal an equilibrium temperature that is not consistent with the known oceanographic conditions of the area, other mechanisms may be invoked. Factors that may affect the isotopic composition by increasing $\delta^{18}O$ values include the mixing of waters originating e.g. from the dissociation of gas hydrates, or from the illitization of clay minerals occurring at depth (Savin and Epstein, 1970; Hesse and Harrison, 1981; Kastner et al., 1993; Aloisi et al., 2000;

Table 4
Main statistical parameters of measured CH_4 and CO_2 flux data from Kalang Anyar MV.

	Mean	Geometric Mean	Median	Minimum	Maximum	Std.Dev.
Flux CO_2 (g $m^{-2}day^{-1}$)	37.88	22.82	20.58	1.18	179.86	41.07
Flux CH_4 (g $m^{-2}day^{-1}$)	64.37	0.15	0.021	0.0005	643.36	151.93

Table 5
Estimated output of φCH_4 and φCO_2 from macro-seeps (measured and estimated) and miniseepage measured in the crater zone and surrounding region from Kalang Anyar MV.

	Crater zone				Surrounding region		
	Macro-seeps		Miniseepage		Miniseepage		
	Range	Mean	Range	Mean	Range	Mean	Total
Flux CH_4 (g $m^{-2}day^{-1}$)	8.03–643.36	277.29	0.02–0.095	0.05	0.0005–0.027	0.01	
Flux CO_2 (g $m^{-2}day^{-1}$)	53–180	92.51	7.82–34.81	19.94	1.18–49.06	18.68	
	Macro-seeps		**Miniseepage**		**Miniseepage**		
	measured	estimated	estimated		estimated		
Flux CH_4 (kg day^{-1})	2.50	13.31	0.98		1.47		
Flux CO_2 (kg day^{-1})	0.85	4.44	-		-		
φCH_4 (t yr^{-1})		4.86	0.36		0.54		5.75
φCO_2 (t yr^{-1})		1.62	-		-		1.62

Dählmann and de Lange, 2003; Mazzini et al., 2016).

Oxygen isotope analyses of the shells and authigenic carbonate cements of Kalang Anyar provide insights into ambient environmental conditions during their precipitation. The carbonates were obtained by drilling of samples and we cannot exclude a partial mixing with older geological carbon, but some main observations may be highlighted. Carbonates from shells reveal $\delta^{18}O$ values significantly lower than those from methanogenic cements (as high as 0.7‰). The oyster shells from Type 2 carbonates have the lowest $\delta^{18}O$ values (as low as −6.2‰). These shells are present on the external part of the blocks, and record the temperature signature of the tropical water from which the carbonates precipitated. In contrast, shells from Type 1 carbonates ($\delta^{18}O = -4.6$‰) may either represent precipitation conditions of deeper (and presumably colder) water or reflect a partial mixing with ^{18}O-enriched seeping fluids. This second scenario is strengthened by the fact that these shells are not colonizing the external surface of the blocks but are rather incorporated within the blocks, indicating that these chemosymbiotic species were thriving at seepage sites during the precipitation of authigenic carbonate. Similarly, the authigenic carbonates appear to have distinct $\delta^{18}O_{VSMOW}$ signatures with Type 1 displaying values as low as −3.3‰. Since there is no consistency with the variations displayed by the shell carbonates, we suggest that these shifts reflect changes in the chemistry of the seeping fluids. In fact, these anomalously high $\delta^{18}O_{VSMOW}$ values would reflect equilibrium temperatures far lower than those present in this tropical setting. In turn, the $\delta^{18}O_{VSMOW}$ results allow us to exclude that these isotopic values are related to the dissociation of gas hydrates, which would not have been stable given the warm water temperatures and relatively shallow water depths inferred at this locality. The high $\delta^{18}O_{VSMOW}$ values are instead consistent with a contribution of fluids originating from the illitization of clay minerals. This conclusion is in good agreement with the oxygen water isotope values of the fluids currently seeping at Kalang Anyar MV with $\delta^{18}O_{VSMOW}$ ranging between 2.5 and 6.2‰ (Mazzini et al., 2018). A similar conclusion has been reached for neighbouring MVs (i.e. Pulungan and Gunung Anyar) based on isotopic analyses of their pore waters (Mazzini et al., 2018).

5.4. Migration of mantle-derived fluids in the sedimentary basin

Studies of seepage sites in the southern part of the East Java Basin (20 km to the SW of Kalang Anyar MV) provide evidence that mantle-derived fluids (e.g. CO_2, He, Rn) are migrating to surface along a broad area of the basin intersected by the Watukosek fault system (Mazzini et al., 2012; Sciarra et al., 2018; Zaputlyaeva et al., 2019). Fig. 7A and B summarises R/Ra and $\delta^{13}C_{-CO2}$ values along a SW-NE oriented section (data compiled from Mazzini et al., 2012; Inguaggiato et al., 2018; Sciarra et al., 2018; Zaputlyaeva et al., 2019). from the Kalang Anyar MV to the Arjuno-Welirang fumaroles. The helium isotopes are essentially stable at 6.5–7 R/Ra up to 27 km from the Welirang fumaroles (considered to be the end-member), while both helium and CO_2 isotopes gradually decrease approaching Kalang Anyar (Fig. 7B). In contrast, evidence of a lesser input of mantle-derived fluids is reported in localities along the western side of the Arjuno-Welirang volcanic complex (i.e. Watudakon field, Zaputlyaeva et al., 2019), confirming that the Watukosek fault system efficiently promotes the migration of volcanic fluids. Helium in the Kalang Anyar MV is characterized by a two-component mixture between crustal and mantle helium (Fig. 7C). A simple mass balance calculation allows us to estimate the mantle-derived helium contribution in the range of 3.8–4.1%, assuming the Welirang fumaroles to be representative of the local MORB composition (R/Ra = 6.5–7). Our helium data reveal that the migration of mantle-derived fluids extends towards the northeast of the volcanic complex, where the WFS hosts the Kalang Anyar MV. A broader sampling is needed to verify if neighbouring MVs also have evidence of mantle-derived He.

Further insights about the lateral migration of volcanic fluids is provided by the comparable ^{13}C enrichment of CO_2 at Kalang Anyar MV ($\delta^{13}C_{CO2}$ as high as −4‰) and at the neighbouring Pulungan and Gunung Anyar MVs ($\delta^{13}C_{CO2}$ as high as −3.8‰, Mazzini et al., 2012). This group of MVs has a gas geochemistry that is comparable with seepage sites located close to the volcanic arc (e.g. Mazzini et al., 2012; Sciarra et al., 2018; Zaputlyaeva et al., 2019) which have values that are consistent with a setting where the main vents are connected to deep-rooted thermogenic methane reservoirs and where the sedimentary volcanism is geothermally perturbed by the migration of mantle-derived fluids (Fig. 7).

Our results support previous proposals of mantle-derived fluid migration through the sedimentary basin along the WFS (Mazzini et al., 2012; Zaputlyaeva et al., 2019). This is also in agreement with recent tomographic studies which show that the eruptive systems in this region of East Java are aligned along a NE-striking direction. Here, fluids capitalise on the enhanced hydraulic transmissivity of the upper crust where the left-lateral WFS intersects the fold and thrust sequence that characterizes the back-arc basin (Lupi et al., 2022).

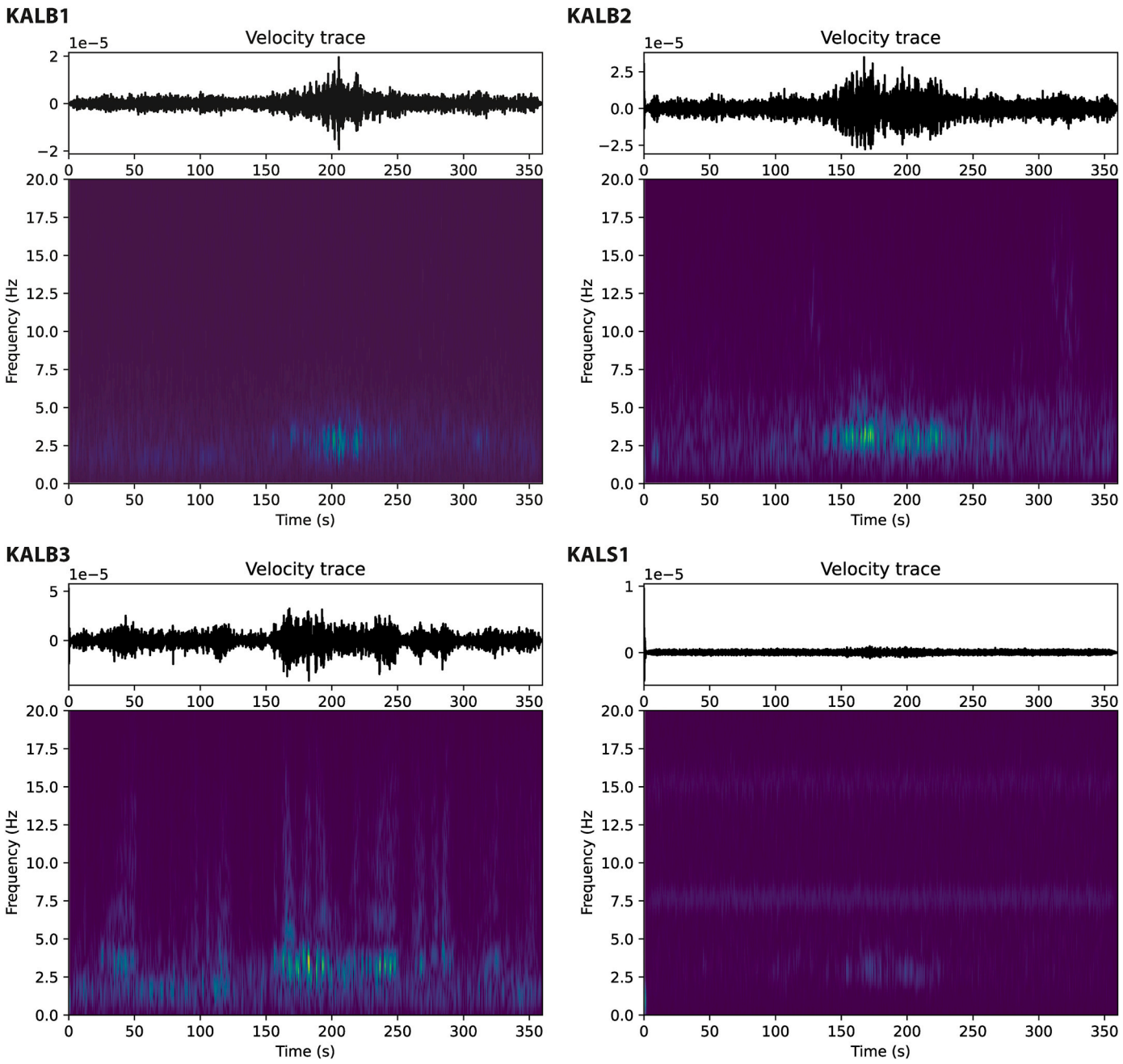

Fig. 6. Drumbeat seismic signal recorded at the 4 seismometers deployed atop Kalang Anyar MV (locations shown in Fig. 5A; coordinates are: KALS1 -7.3996–112.7887, KALB1 -7.4003–112.7901, KALB2 -7.3991–112.7896, KALB3 -641 7.4002–112.7889). At all stations, the top panel records (Top Traces) show the occurrence of an emergent signal lasting about 100 s (velocity is reported in m/s). The bottom panels show the spectrograms (bandpassed between 1 Hz and 18 Hz) characterized by dominant frequencies of 3–4 Hz and high frequencies up to 15 Hz. The signal appears simultaneously on the 4 stations but drastically decays on the station further away from the main vent region.

5.5. *Comparison of flux styles and rates*

A profile of CH_4 and CO_2 flux across Kalang Anyar MV reveals methane-dominated diffused degassing with distinctly higher rates in the summit crater area compared with the surrounding region (Fig. 5A and B). This observation is common at MV sites where advective fluid migration typically occurs at and around the crater and more specifically at seepage sites where gas leakage is determined by pressure gradient and rock permeability (e.g. Etiope, 2015 and refs therein), whereas in surrounding areas diffusive flux prevails at outward decreasing rates. In order to assess the degassing magnitude of Kalang Anyar MV, we compared our results for total methane emission with that of other structures of similar or smaller size. Among these, MVs that are considered to have low emission rates include Kamou -Japan; Frisa, Pineto, Nirano -Italy; Lokbatan -Azerbaijan; Andreiasu, Lepsa, Sacelu-Gori, and Raiuti -Romania, which have CH_4 flow rates in the range of 0.03–6.85 t yr^{-1} (Mazzini et al., 2021a and refs therein). Similar sized MVs with high emission rates include: Murono -Japan; Regnano -Italy; Monor, Beciu, Paclele Mici, Lopatari, Alimpesti -Romania; Wu-shan-ding, Dushanzi -China, which degas from 16 to 383 t yr^{-1} CH_4 (Mazzini et al., 2021a and refs therein). Our results indicate that Kalang Anyar MV degasses 5.75 t yr^{-1} of CH_4 and can therefore be considered as a low emitter overall.

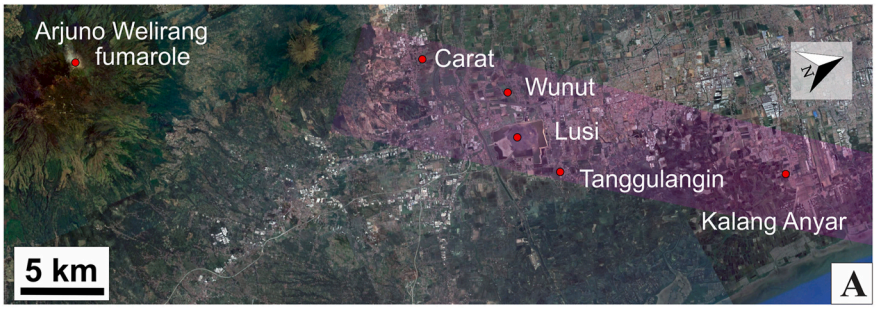

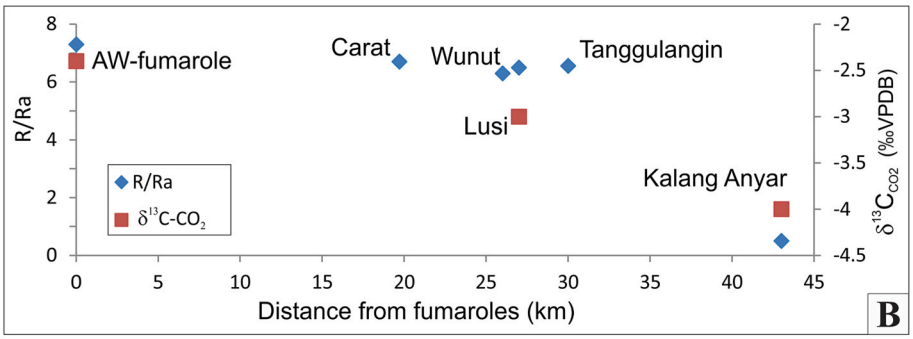

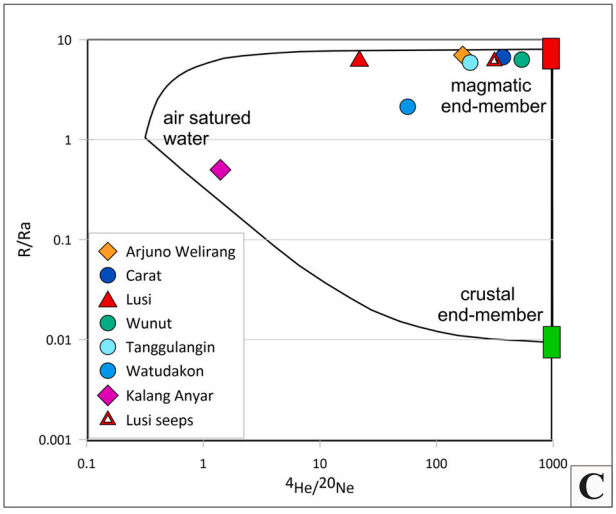

Fig. 7. Evidence of migration of mantle-derived fluids through the sedimentary basin. (A) Google Earth satellite image of north-east Java indicating gas sampling localities along a W-E profile across the Watukosek fault system (purple shaded area), from the Arjuno-Welirang volcanic complex at left (reference sample at the fumaroles), to the sedimentary basin at the right. (B): R/Ra and $\delta^{13}C_{CO2}$ values from the sample locations shown in A, revealing a gradual decrease of mantle-derived fluid components away from Arjuno-Welirang towards the NE part of the sedimentary basin. (C) He isotope ratios versus $^{4}He/^{20}Ne$ ratios for emitted fluids in the Arjuno-Welirang volcanic complex, gas fields (Carat, Wunut, Tanggulangin and Watudakon), Lusi and Kalang Anyar MV. The lines represent the theoretical mixing curves of atmospheric helium with crustal and with mantle-originated helium. The end-members atmosphere/crust/mantle are shown for reference. New data from this article are compiled with previously published analyses (Mazzini et al., 2012; Inguaggiato et al., 2018; Sciarra et al., 2018; Zaputlyaeva et al., 2019). (For interpretation of the references to colour in this figure legend, the reader is referred to the Web version of this article.)

5.6. Drumbeat seismic signal

A seismic signal similar to the one observed at Kalang Anyar MV has been described by Lupi et al. (2016) and Antunes et al. (2022) at the Nirano MV in Italy. The authors note that the signal may consist mainly of P-waves released at shallow depths or generated inside the mud-conduit by rising bubbles. While drag-forces due to gas migration may indeed generate drumbeat signals, rising and collapsing bubbles should generate some sort of acoustic waves that we do not observe in our record. Instead, we argue that the high-frequency signals observed at Kalang Anyar MV, which last up to 3 min, may be generated within the narrow conduits of mud volcanoes. In particular, we propose that the drumbeat signal observed at Kalang Anyar and other MVs may be caused by bottle-neck structures at the intersection between the shallow mud reservoir and the sub-vertical conduit of the mud edifice. Here, gas phases that mingled inside the liquid mud may upwell driven by pressure and enter shallow subvertical conduits forming pathways through a highly fractured geological media. Previous authors (Mazzini and Etiope, 2017; Antunes et al., 2022; Giambastiani et al., Under review) argue for the occurrence of a semi-liquid shallow reservoir below mud volcanoes. The intersection of such a shallow reservoir with subvertical conduits may be the region from which drumbeat seismic signals originate.

5.7. Mud volcanism and geohazards

A comparison of images from Google Earth during the last 15 years (Fig. 8A–J) reveals an impressive increase in human constructions around and within the active crater zone of Kalang Anyar MV. The constructions include residences and industrial infrastructures. This uncontrolled urban expansion poses a serious hazard for people and infrastructures in the area, especially when these edifices are alarmingly close to active seepage sites (Fig. 2G). The observation of clasts of differing lithologies and sizes within the mud breccia flows indicates that episodic eruptive events were sufficiently powerful to extrude to the surface rock fragments from the geological units and formations pierced by the mud volcano conduit. Although these factors have often been overlooked, in several cases MVs have proven to be dangerous natural phenomena that impact human communities, even causing the loss of lives. Historical records of recent destructive events are available from Azerbaijan, China, Russia, Italy, Taiwan, Trinidad (e.g., Mazzini and Etiope, 2017 and refs therein). This type of geohazard is exacerbated on

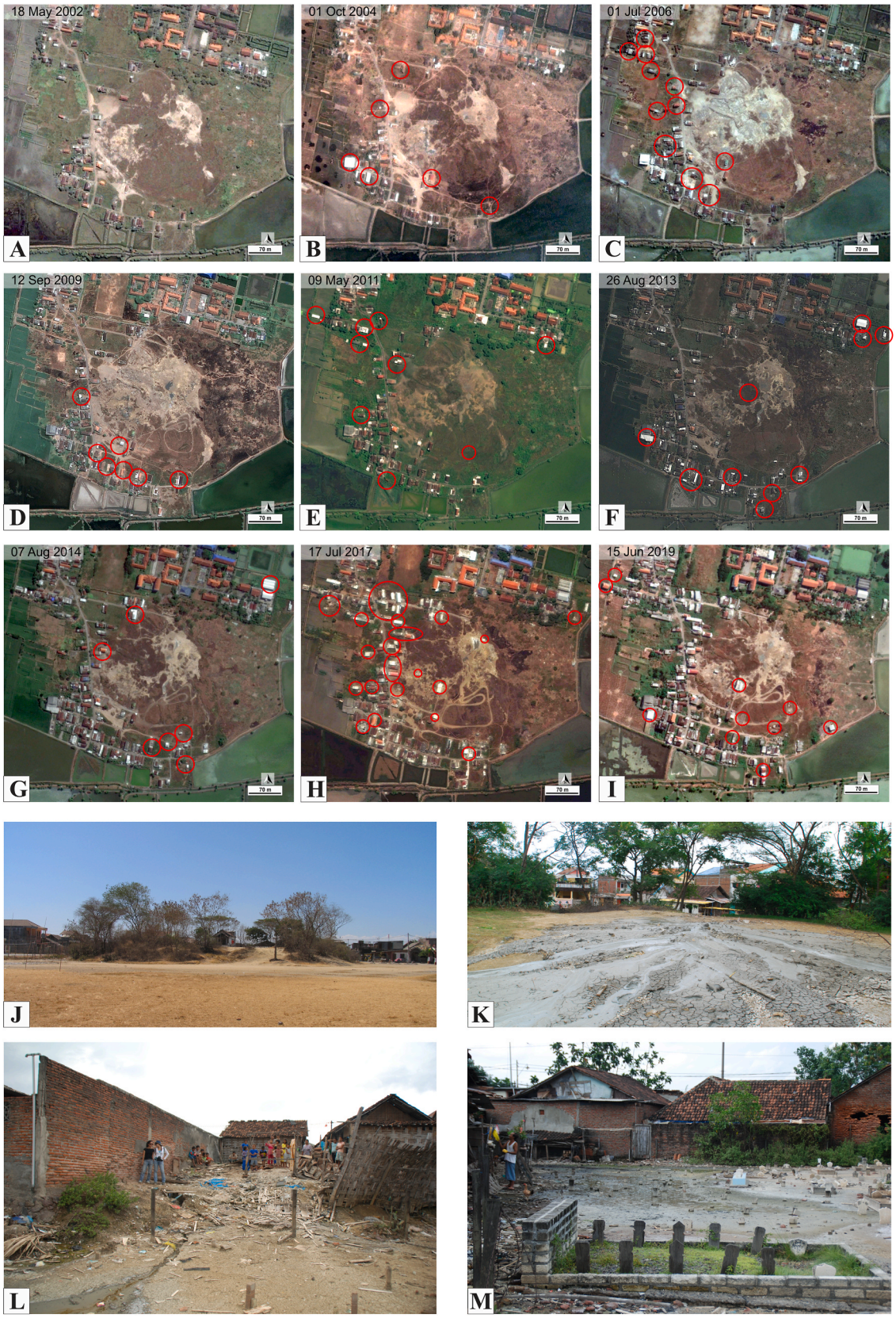

Fig. 8. Mud volcanoes and geohazards in Java. (A–I) Google Earth images of Kalang Anyar MV from 2002 to 2019. In each image are circled (in red) constructions that are new relative to the previous satellite image; (J–K) Photos of Gunung Anyar MV (2006) surrounded by houses very close to the crater where active seepage is ongoing; (L–M) photos of Pulungan MV (2006) is entirely covered by settlements that were damaged after its 2006 activity. (For interpretation of the references to colour in this figure legend, the reader is referred to the Web version of this article.)

the island of Java due to its dense population. Among numerous examples, we cite the neighbouring Polungan and Gunung Anyar MVs, where congested settlements are either framing or completely covering the craters of these structures (Fig. 8K-M). To date the most recent Indonesian MV eruptions took place at Kesongo MV (central Java, Blora Regency) on the August 27, 2020 and again on the December 3, 2021, when sudden mud blasts reached tens of meters in height and extended over hundreds of square meters, injuring four people and resulting in the loss of herds of buffaloes (The Watchers, 2022).

6. Conclusions

We present the results of a multidisciplinary study of Kalang Anyar mud volcano, based on geological and geophysical field observations integrated with geochemical analyses of samples of erupted fluids and associated methanogenic carbonates. Gas geochemistry shows that the numerous seepage sites scattered within the crater are methane-dominated with a strong thermogenic component. CO_2 isotopes indicate the presence of mantle-derived fluids that rise to surface through this part of the sedimentary basin, suggesting that the influence of the Arjuno-Welirang volcanic complex extends to the north-east of the Java Island. Overall our geochemical results support a scenario in which the migration of fluids is promoted by the intersection of the Watukosek fault system with the low angle thrust faults generated during compressional tectonics in this back-arc basin. A similar mechanism is expected for neighbouring mud volcanoes. Seismometer records reveal the occurrence of a drumbeat signal which we propose to be produced by the migration of fluids across the shallow plumbing system.

Well-preserved shells scattered across the mud volcano site indicate that the area was once located below the seal level. Carbonate blocks located on the outskirts of the crater zone have a methanogenic origin and were formed by microbially-mediated methane oxidation and carbonate precipitation during the submarine activity of the mud volcano. These blocks contain densely packed vesicomyds or are covered on their external surface by oyster shells that date the emergence of the MV from the sea to the last 2 ka. Similar carbonate deposits are broadly documented from modern and fossil offshore seepage sites. Kalang Anyar represents a rare example of an onshore mud volcano that has previously experienced submarine activity and associated precipitation of authigenic carbonates.

Mud breccia flows containing a mixture of clasts of differing lithologies and sizes cover a total area of ~1.5 km^2. This suggests that powerful eruptions were able to eject clasts from the various formations intersected by the mud volcano conduit. Today, the surface of the mud volcano is largely populated and exponentially growing construction may pose a severe danger for residents in case of sudden eruptive activity. Uncontrolled development at this and other active mud volcanoes is common and represents a clear geohazard that is often neglected.

Declaration of competing interest

The authors declare that they have no known competing financial interests or personal relationships that could have appeared to influence the work reported in this paper.

Data availability

Data will be made available on request.

Acknowledgments

This study was funded by the European Research Council under the European Union's Seventh Framework Program Grant agreement no 308126 (Lusi LAB project, PI A. Mazzini). We acknowledge the support of the Research Council of Norway (NFR) through the HOTMUD project number 288299 and its centers of Excellence funding scheme, project number 223272 (CEED). Matteo Lupi was supported by an Swiss National Science Foundation, Ambizione grant (project n° 154815). We thank Francisco J. Munoz Burbano for the support with Fig. 6 and Clint Conrad for his useful comments. The editor and two anonymous reviewers are thanked for their constructive reviews.

References

Akhmanov, G.G., Premoli Silva, I., Erba, E., Cita, M.B., 2003. Sedimentary succession and evolution of the Mediterranean Ridge western sector as derived from lithology of mud breccia clasts. Mar. Geol. 195 (1–4), 277–299.
Albarello, D., Palo, M., Martinelli, G., 2012. Monitoring methane emission of mud volcanoes by seismic tremor measurements: a pilot study: Nat. Hazards Earth Syst. Sci. 12 (12), 3617–3629.
Aloisi, G., Pierre, C., Rouchy, J.M., Foucher, J.P., Woodside, J., 2000. Methane-related authigenic carbonates of eastern Mediterranean Sea mud volcanoes and their possible relation to gas hydrate destabilisation. Earth Planet Sci. Lett. 184 (1), 321–338.
Antunes, V., Planes, R., Obermann, A., Panzera, F., d'Amico, S., AM, sciarra, A., Ricci, T., Lupi, M., 2022. Insights into the dynamics of the nirano mud volcano through seismic characterization of drumbeat signals and V/H analysis. J. Volcanol. Geoth. Res. 431, 107619.
Baldocchi, D.D., Meyers, T.P., 1991. Trace gas exchange above the floor of a deciduous forest: 1. Evaporation and CO2 efflux. J. Geophys. Res. Atmos. 96 (D4), 7271–7285.
Boetius, A., Ravenschlag, K., Schubert, C.J., Rickert, D., Widdel, F., Gieseke, A., Amann, R., Jorgensen, B.B., Witte, U., Pfannkuche, O., 2000. A marine microbial consortium apparently mediating anaerobic oxidation of methane. Nature 407, 623–625.
Boetius, A., Wenzhofer, F., 2013. Seafloor oxygen consumption fuelled by methane from cold seeps. Nat. Geosci. 6 (9), 725–734.
Campbell, K.A., Nelson, C.S., Alfaro, A.C., Boyd, S., Greinert, J., Nyman, S., Grosjean, E., Logan, G.A., Gregory, M.R., Cooke, S., Linke, P., Milloy, S., Wallis, I., 2010. Geological imprint of methane seepage on the seabed and biota of the convergent Hikurangi Margin, New Zealand: box core and grab carbonate results. Mar. Geol. 272 (1), 285–306.
Chiodini, G., Frondini, F., 2001. Carbon dioxide degassing from the Albani Hills volcanic region. Central Italy: Chem. Geol. 177, 67–83.
Clements, B., Hall, R., Smyth, H.R., Cottam, M.A., 2009. Thrusting of a volcanic arc: a new structural model for Java. Petrol. Geosci. 15 (2), 159–174.
Collignon, M., Mazzini, A., Schmid, D.W., Lupi, M., 2018. Modelling fluid flow in active clastic piercements: challenges and approaches. Mar. Petrol. Geol. 90, 157–172.
Cordes, E.E., Bergquist, D.C., Fisher, C.R., 2009. Macro-ecology of gulf of Mexico cold seeps. Ann. Rev. Mar. Sci 1 (1), 143–168.
Cordes, E.E., Cunha, M.R., Galéron, J., Mora, C., Olu-Le Roy, K., Sibuet, M., Van Gaever, S., Vanreusel, A., Levin, L.A., 2010. The influence of geological, geochemical, and biogenic habitat heterogeneity on seep biodiversity. Mar. Ecol. 31 (1), 51–65.
Cunha, M.R., Rodrigues, C.F., Génio, L., Hilário, A., Ravara, A., Pfannkuche, O., 2013. Macrofaunal assemblages from mud volcanoes in the Gulf of Cadiz: abundance, biodiversity and diversity partitioning across spatial scales. Biogeosciences 10 (4), 2553–2568.
Dählmann, A., de Lange, G.J., 2003. Fluid–sediment interactions at Eastern Mediterranean mud volcanoes: a stable isotope study from ODP Leg 160. Earth Planet Sci. Lett. 212 (3–4), 377–391.
Di Felice, F., Mazzini, A., Di Stefano, G., Romeo, G., 2018. Drone high resolution infrared imaging of the Lusi mud eruption. Mar. Petrol. Geol. 90, 38–51.
Di Stefano, G., Romeo, G., Mazzini, A., Iarocci, A., Hadi, S., Pelphrey, S., 2018. The Lusi drone: a multidisciplinary tool to access extreme environments. Mar. Petrol. Geol. 90, 26–37.
Doust, H., Noble, R.A., 2008. Petroleum systems of Indonesia. Mar. Petrol. Geol. 25 (2), 103–129.
Dupré, S., Woodside, J., Klaucke, I., Mascle, J., Foucher, J.-P., 2010. Widespread active seepage activity on the Nile Deep Sea Fan (offshore Egypt) revealed by high-definition geophysical imagery. Mar. Geol. 275 (1–4), 1–19.
Etiope, G., 2015. Natural Gas Seepage. The Earth's Hydrocarbon Degassing. Springer International Publishing Switzerland, ISBN 978-3-319-14601-0, p. 199 (eBook).
Fallahi, M.J., Obermann, A., Lupi, M., Karyono, K., Mazzini, A., 2017. The plumbing system feeding the Lusi eruption revealed by ambient noise tomography. J. Geophys. Res. Solid Earth 122 (10), 8200–8213.
Gattuso, A., Italiano, F., Capasso, G., D'Alessandro, A., Grassa, F., Pisciotta, A.F., Romano, D., 2021. The mud volcanoes at Santa Barbara and Aragona (Sicily, Italy): a contribution to risk assessment: Nat. Hazards Earth Syst. Sci. 21 (11), 3407–3419.
Giambastiani, B.M.S., Antonellini, M., Nespoli, M., Bacchetti, M., Calafato, A., Conventi, M., Dadomo, A., Martinelli, G., Morena, M., Venturoli, S., Piombo, A., 2021. Mud flow dynamics at gas seeps - nirano Salse, Italy. Environ. Earth Sci. 81 (19) (2022/10/01 2022): 480.
Gunawan, E., Widiyantoro, S., 2019. Active tectonic deformation in Java, Indonesia inferred from a GPS-derived strain rate. J. Geodyn. 123, 49–54.
Hall, R., Clements, B., Smyth, H.R., Cottam, M.A., 2007. A new interpretation of Java's structure. In: Indonesian Petroleum Association, Proceedings 31st Annual Convention, pp. 63–86, 2007.
Hatem, E., Tribovillard, N., Averbuch, O., Vidier, D., Sansjofre, P., Birgel, D., Guillot, F., 2014. Oyster patch reefs as indicators of fossil hydrocarbon seeps induced by synsedimentary faults. Mar. Petrol. Geol. 55, 176–185.

Hesse, R., Harrison, W., 1981. Gas hydrates (clathrates) causing pore-water freshening and oxygen isotope fractionation in deep-water sedimentary section of terrigenous continental margins. Earth Planet Sci. Lett. 55, 453–462.
Hogg, A.G., Heaton, T.J., Hua, Q., Palmer, J.G., Turney, C.S., Southon, J., Bayliss, A., Blackwell, P.G., Boswijk, G., Ramsey, C.B., Pearson, C., Petchey, F., Reimer, P., Reimer, R., Wacker, L., 2020. SHCal20 Southern Hemisphere calibration, 0–55,000 years cal BP. Radiocarbon 62 (4), 759–778.
Hovland, M., Judd, A.G., 1988. Seabed Pockmarks and Seepages: Impact on Geology, Biology and the Marine Environment. Graham & Trotman, p. 293.
Inguaggiato, S., Mazzini, A., Vita, F., Sciarra, A., 2018. The Arjuno-Welirang volcanic complex and the connected Lusi system: geochemical evidences. Mar. Petrol. Geol. 90, 67–76.
Istadi, B., Wibowo, H.T., Sunardi, E., Hadi, S., Sawolo, N., 2012. Mud Volcano and its Evolution: in Tech, ISBN 978-953-307-861-8, pp. 375–434.
Ivanov, M., Mazzini, A., Blinova, V., Kozlova, E., Laberg, J.-S., Matveeva, T., Taviani, M., Kaskov, N., 2010. Seep mounds on the southern vøring plateau (offshore Norway). Mar. Petrol. Geol. 27 (6), 1235–1261.
Judd, A., Noble-James, T., Golding, N., Eggett, A., Diesing, M., Clare, D., Silburn, B., Duncan, G., Field, L., Milodowski, A., 2020. The Croker Carbonate Slabs: extensive methane-derived authigenic carbonate in the Irish Sea—nature, origin, longevity and environmental significance. Geo Mar. Lett. 40 (4), 423–438.
Karyono, K., Obermann, A., Lupi, M., Masturyono, M., Hadi, S., Syafri, I., Abdurrokhim, A., Mazzini, A., 2017. Lusi, a clastic-dominated geysering system in Indonesia recently explored by surface and subsurface observations. Terra. Nova 29 (1), 13–19.
Kastner, M., Elderfield, H., Jenkins, W.J., Gieskes, J.M., Gamo, T., 1993. Geochemical and isotopic evidence for fluid flow in the western nankai subduction zone, Japan. Proc. Ocean Drill. Progr. Sci. Results 131, 397–413.
Levin, L.A., Baco, A.R., Bowden, D.A., Colaco, A., Cordes, E.E., Cunha, M.R., Demopoulos, A.W.J., Gobin, J., Grupe, B.M., Le, J., Metaxas, A., Netburn, A.N., Rouse, G.W., Thurber, A.R., Tunnicliffe, V., Van Dover, C.L., Vanreusel, A., Watling, L., 2016. Hydrothermal vents and methane seeps: rethinking the sphere of influence. Front. Mar. Sci. 3 (72).
Lupi, M., De Gori, P., Valoroso, L., Baccheschi, P., Minetto, R., Mazzini, A., 2022. Northward migration of the Javanese volcanic arc along thrust faults. Earth Planet Sci. Lett. 577, 117258.
Lupi, M., Ricci, B.S., Kenkel, J., Ricci, T., Fuchs, F., Miller, S.A., Kemna, A., 2016. Subsurface fluid distribution and possible seismic precursory signal at the Salse di Nirano mud volcanic field. Italy: Geophys. J. Int. 204 (2), 907–917.
Lupi, M., Saenger, E.H., Fuchs, F., Miller, S.A., 2013. Lusi mud eruption triggered by geometric focusing of seismic waves. Nat. Geosci. 6 (8), 642–646.
Lupi, M., Sciarra, A., Mazzin, A., Carrier, A., Husein, A., Karyono, K., 2018. Geophysical and Soil Degassing Observations at the Kalang Anyar Mud Volcano, East Java, EGU General Assembly Conference Abstracts, 13402. April 01, 2018.
Magalhães, V.H., Pinheiro, L.M., Ivanov, M.K., Kozlova, E., Blinova, V., Kolganova, J., Vasconcelos, C., McKenzie, J.A., Bernasconi, S.M., Kopf, A.J., Díaz-del-Río, V., González, F.J., Somoza, L., 2012. Formation processes of methane-derived authigenic carbonates from the Gulf of Cadiz. Sediment. Geol. 243–244, 155–168.
Mann, T., Bender, M., Lorscheid, T., Stocchi, P., Vacchi, M., Switzer, A.D., Rovere, A., 2019. Holocene sea levels in Southeast Asia, Maldives, India and Sri Lanka: the SEAMIS database. Quat. Sci. Rev. 219, 112–125.
Manton, B., Müller, P., Mazzini, A., Zastrozhnov, D., Jerram, D.A., Millett, J.M., Schmid, D.W., Berndt, C., Myklebust, R., Planke, S., 2022. Characterizing ancient and modern hydrothermal venting systems. Mar. Geol. 447, 106781.
Mauri, G., Husein, A., Mazzini, A., Irawan, D., Sohrabi, R., Hadi, S., Prasetyo, H., Miller, S.A., 2018a. Insights on the structure of Lusi mud edifice from land gravity data. Mar. Petrol. Geol. 90, 104–115.
Mauri, G., Husein, A., Mazzini, A., Karyono, K., Obermann, A., Bertrand, G., Lupi, M., Prasetyo, H., Hadi, S., Miller, S.A., 2018b. Constraints on density changes in the funnel-shaped caldera inferred from gravity monitoring of the Lusi mud eruption. Mar. Petrol. Geol. 90, 91–103.
Mazzini, A., Akhmanov, G., Manga, M., Sciarra, A., Huseynova, A., Huseynov, A., Guliyev, I., 2021a. Explosive mud volcano eruptions and rafting of mud breccia blocks. Earth Planet Sci. Lett. 555, 116699.
Mazzini, A., Carrier, A., Sciarra, A., Fischanger, F., Winarto-Putro, A., Lupi, M., 2021b. 3D deep electrical resistivity tomography of the Lusi eruption site in east Java. Geophys. Res. Lett. 48 (18), e2021GL092632.
Mazzini, A., Etiope, G., 2017. Mud volcanism: an updated review. Earth Sci. Rev. 168, 81–112.
Mazzini, A., Etiope, G., Svensen, H., 2012. A new hydrothermal scenario for the 2006 Lusi eruption, Indonesia. Insights from gas geochemistry. Earth Planet Sci. Lett. 317, 305–318.
Mazzini, A., Ivanov, M.K., Nermoen, A., Bahr, A., Bohrmann, G., Svensen, H., Planke, S., 2008. Complex plumbing systems in the near subsurface: geometries of authigenic carbonates from Dolgovskoy Mound (Black Sea) constrained by analogue experiments. Mar. Petrol. Geol. 25 (6), 457–472.
Mazzini, A., Ivanov, M.K., Parnell, J., Stadnitskaia, A., Cronin, B.T., Poludetkina, E., Mazurenko, L., van Weering, T.C.E., 2004. Methane-related authigenic carbonates from the Black Sea: geochemical characterisation and relation to seeping fluids. Mar. Geol. 212 (1–4), 153–181.
Mazzini, A., Nermoen, A., Krotkiewski, M., Podladchikov, Y., Planke, S., Svensen, H., 2009. Strike-slip faulting as a trigger mechanism for overpressure release through piercement structures. Implications for the Lusi mud volcano, Indonesia: Mar. Petrol. Geol. 26 (9), 1751–1765.
Mazzini, A., Scholz, F., Svensen, H.H., Hensen, C., Hadi, S., 2018. The geochemistry and origin of the hydrothermal water erupted at Lusi, Indonesia. Mar. Petrol. Geol. 90, 52–66.
Mazzini, A., Sciarra, A., Etiope, G., Sadavarte, P., Houweling, S., Pandey, S., Husein, A., 2021c. Relevant methane emission to the atmosphere from a geological gas manifestation. Sci. Rep. 11 (1), 4138.
Mazzini, A., Svensen, H., Akhmanov, G.G., Aloisi, G., Planke, S., Malthe-Sorenssen, A., Istadi, B., 2007. Triggering and dynamic evolution of the LUSI mud volcano, Indonesia. Earth Planet Sci. Lett. 261 (3–4), 375–388.
Mazzini, A., Svensen, H., Hovland, M., Planke, S., 2006. Comparison and implications from strikingly different authigenic carbonates in a Nyegga complex pockmark, G11, Norwegian Sea. Mar. Geol. 231, 89–102.
Mazzini, A., Svensen, H.H., Planke, S., Forsberg, C.F., Tjelta, T.I., 2016. Pockmarks and methanogenic carbonates above the giant Troll gas field in the Norwegian North Sea. Mar. Geol. 373, 26–38.
Michaelis, W., Seifert, R., Nauhaus, K., Treude, T., Thiel, V., Blumenberg, M., Knittel, K., Gieseke, A., Peterknecht, K., Pape, T., Boetius, A., Amann, R., Jørgensen, B., Widdel, F., Peckmann, J., Pimenov, N.V., Gulin, M.B., 2002. Microbial reefs in the Black Sea fueled by anaerobic oxidation of methane. Science 297, 1013–1015.
Miller, S.A., Mazzini, A., 2018. More than ten years of Lusi: a review of facts, coincidences, and past and future studies. Mar. Petrol. Geol. 90, 10–25.
Minetto, R., Montanari, D., Planès, T., Bonini, M., Del Ventisette, C., Antunes, V., Lupi, M., 2020. Tectonic and anthropogenic microseismic activity while drilling toward supercritical conditions in the larderello-travale geothermal field, Italy. J. Geophys. Res. Solid Earth 125 (2), e2019JB018618.
Mitrovica, J.X., Milne, G.A., 2002. On the origin of late Holocene sea-level highstands within equatorial ocean basins. Quat. Sci. Rev. 21 (20–22), 2179–2190.
Mitrovica, J.X., Peltier, W.R., 1991. On postglacial geoid subsidence over the equatorial oceans. J. Geophys. Res. Solid Earth 96 (B12), 20053–20071.
Moscariello, A., Do Couto, D., Mondino, F., Booth, J., Lupi, M., Mazzini, A., 2018. Genesis and evolution of the Watukosek Fault system in the Lusi area (east Java). Mar. Petrol. Geol. 90, 125–137.
Mudjiono, R., Pireno, G.E., 2002. Exploration Madura platform, offshore, East Java, Indonesia, pp. 707e726 Indonesia Petroleum Association Proceedings 28 (1), 707–7269.
Naehr, T.H., Eichhubl, P., Orphan, V.J., Hovland, M., Paull, C.K., Ussler, W., Lorenson, T. D., Greene, H.G., 2007. Authigenic carbonate formation at hydrocarbon seeps in continental margin sediments: a comparative study: deep Sea Research Part II. Topical Studies in Oceanography 54 (11), 1268–1291.
Norman, J.M., Garcia, R., Verma, S.B., 1992. Soil surface CO2 fluxes and the carbon budget of a grassland. J. Geophys. Res. Atmos. 97 (D17), 18845–18853.
Novianto, A., Sutanto, Suharsono, Prasetyadi, C., Setiawan, T., 2020. Structural model of kendeng basin: a new concept of oil and gas exploration. Open Journal of Yangtze Oil and Gas 5, 200–215.
Obermann, A., Karyono, K., Diehl, T., Lupi, M., Mazzini, A., 2018. Seismicity at Lusi and the adjacent volcanic complex, Java, Indonesia. Mar. Petrol. Geol. 90, 149–156.
Osorio Riffo, Á., Mauri, G., Mazzini, A., Miller, S.A., 2021. Tectonic insight and 3-D modelling of the Lusi (Java, Indonesia) mud edifice through gravity analyses. Geophys. J. Int. 225 (2), 984–997.
Pierre, C., Bayon, G., Blanc-Valleron, M.-M., Mascle, J., Dupré, S., 2014. Authigenic carbonates related to active seepage of methane-rich hot brines at the Cheops mud volcano, Menes caldera (Nile deep-sea fan, eastern Mediterranean Sea). Geo Mar. Lett. 34 (2), 253–267.
Ramsey, C.B., 1995. Radiocarbon calibration and analysis of stratigraphy: the OxCal program. Radiocarbon 37 (2), 425–430.
Reimer, P.J., Austin, W.E.N., Bard, E., Bayliss, A., Blackwell, P.G., Ramsey, C.B., Butzin, M., Cheng, H., Edwards, R.L., Friedrich, M., Grootes, P.M., Guilderson, T.P., Hajdas, I., Heaton, T.J., Hogg, A.G., Hughen, K.A., Kromer, B., Manning, S.W., Muscheler, R., Palmer, J.G., Pearson, C., van der Plicht, J., Reimer, R.W., Richards, D.A., Scott, E.M., Southon, J.R., Turney, C.S.M., Wacker, L., Adolphi, F., Buntgen, U., Capano, M., Fahrni, S.M., Fogtmann-Schulz, A., Friedrich, R., Kohler, P., Kudsk, S., Miyake, F., Olsen, J., Reinig, F., Sakamoto, M., Sookdeo, A., Talamo, S., 2020. The Intcal20 northern hemisphere radiocarbon age calibration curve (0-55 cal kbp). Radiocarbon 62 (4), 725–757.
Ritt, B., Pierre, C., Gauthier, O., Wenzhofer, F., Boetius, A., Sarrazin, J., 2011. Diversity and distribution of cold-seep fauna associated with different geological and environmental settings at mud volcanoes and pockmarks of the Nile Deep-Sea Fan. Mar. Biol. 158 (6), 1187–1210.
Sano, Y., Wakita, H., 1988. Precise measurement of helium-isotopes in terrestrial gases. Bull. Chem. Soc. Jpn. 61 (4), 1153–1157.
Satyana, A.H., Asnidar, A., 2008. Mud diapirs and mud volcanoes in depressions of Java to Madura: origins, natures, and implications to petroleum system. IPA 32nd Annual Convention Proceedings IPA08-G-139, 1–34.
Satyana, A.H., Darwis, A., 2001. Recent significant discoveries within oligo-miocene carbonates of the east Java basin : integrating the petroleum geology. Proceedings Indonesian Petroleum Association, 30th Annual Conference, September 2001 1–9.
Satyana, A.H., Erwanto, E., Prasetyadi, C., 2004. Rembang-madura-kangean-sakala (RMKS) fault zone, east Java basin: the origin and nature of A geologic border. In: Proc. IAGI, 33rd., Ann. Conv. And Exh., Bandung, 29 NOVEMBER – 1 DECEMBER 2004, pp. 1–23.
Satyana, A.H., Purwaningsih, M.E.M., 2003. Geochemistry of the East Java Basin: New Observations on Oil Grouping, Genetic Gas Types and Trends of Hydrocarbon Habitats: Proceedings Indonesian Petroleum Association, 29th Annual Convention and Exhibition. October 2003. IPA03-G-021.
Savin, S.M., Epstein, S., 1970. The oxygen and hydrogen isotope geochemistry of clay minerals. Geochem. Cosmochim. Acta 34 (1), 25–42.

Sciarra, A., Mazzini, A., Inguaggiato, S., Vita, F., Lupi, M., Hadi, S., 2018. Radon and carbon gas anomalies along the Watukosek Fault System and Lusi mud eruption, Indonesia. Mar. Petrol. Geol. 90, 77–90.

Sibuet, M., Olu, K., 1998. Biogeography, biodiversity and fluid dependence of deep-sea cold-seep communities at active and passive margins. In: Smith, C.R., Mullineaux, L. S., Levin, L.A. (Eds.), Deep-Sea Biodiversity: A Compilation of Recent Advances in Honor of Robert R. Hessler, vol. 45. Elsevier, pp. 517–567. Number 1/3.

Southon, J., Kashgarian, M., Fontugne, M., Metivier, B., Yim, W.W.S., 2002. Marine reservoir corrections for the Indian Ocean and southeast Asia. Radiocarbon 44 (1), 167–180.

The Watchers, 2022. Eruption of Kesongo Mud Volcano in central Java, Indonesia. The Watckers v.

Valentine, D.L., Reeburgh, W.S., 2000. New perspectives on anaerobic methane oxidation. Environ. Microbiol. 2 (5), 477–484.

Van den Bergh, G.D., De Vos, J., Sondaar, P.Y., Aziz, F., 1996. Pleistocene zoogeographic evolution of Java (Indonesia) and glacio-eustatic sea level fluctuations: a background for the presence of Homo. Bulletin of the Indo-Pacific Prehistory Association 14, 7–21.

Vanneste, H., Kastner, M., James, R.H., Connelly, D.P., Fisher, R.E., Kelly-Gerreyn, B.A., Heeschen, K., Haeckel, M., Mills, R.A., 2012. Authigenic carbonates from the Darwin Mud Volcano, Gulf of Cadiz: a record of palaeo-seepage of hydrocarbon bearing fluids. Chem. Geol. 300–301, 24–39.

Vanreusel, A., Andersen, A.C., Boetius, A., Connelly, D., Cunha, M., Decker, C., Hilario, A., Kormas, K.A., Maignien, L., Olu, K., Pachiadaki, M., Ritt, B., Rodrigues, C., Sarrazin, J., Tyler, P.A., Van, G.S., Vanneste, H., 2009. Biodiversity of cold seep ecosystems along the European margins. Oceanography 22 (1), 110–127.

Ward, G.K., Wilson, S.R., 1978. Procedured for comparing and combining radiocarbon age determinations: a critique. Archaeometry 20 (1), 19–31.

Zaputlyaeva, A., Mazzini, A., Blumenberg, M., Scheeder, G., Kürschner, W.M., Kus, J., Jones, M.T., Frieling, J., 2020. Recent magmatism drives hydrocarbon generation in north-east Java, Indonesia. Sci. Rep. 10 (1), 1786.

Zaputlyaeva, A., Mazzini, A., Caracausi, A., Sciarra, A., 2019. Mantle-derived fluids in the east Java sedimentary basin, Indonesia. J. Geophys. Res. Solid Earth 124 (8), 7962–7977.